Remote Sens. **2014**, *6*, 4998-5018; doi:10.3390/rs6064998

OPEN ACCESS

remote sensing

ISSN 2072-4292

www.mdpi.com/journal/remotesensing

Article

Characterization of Drought Development through Remote Sensing: A Case Study in Central Yunnan, China

Sawaid Abbas [1], Janet E. Nichol [1,*], Faisal M. Qamer [2] and Jianchu Xu [3]

[1] Department of Land Surveying and Geo-Informatics, The Hong Kong Polytechnic University, Kowloon, Hong Kong; E-Mail: sawaid.abbas@gmail.com

[2] International Center for Integrated Mountain Development (ICIMOD), Kathmandu 44700, Nepal; E-Mail: fqamer@icimod.org

[3] World Agroforestry Center, East and Central Asia, Kunming 650201, China; E-Mail: j.c.xu@cgiar.org

***** Author to whom correspondence should be addressed; E-Mail: lsjanet@polyu.edu.hk; Tel.: +1-852-2766-5952; Fax: +1-852-2330-2994.

Received: 18 February 2014; in revised form: 19 May 2014 / Accepted: 19 May 2014 / Published: 30 May 2014

Abstract: This study assesses the applicability of remote sensing data for retrieval of key drought indicators including the degree of moisture deficiency, drought duration and areal extent of drought within different land cover types across the landscape. A Normalized Vegetation Supply Water Index (NVSWI) is devised, combining remotely sensed climate data to retrieve key drought indicators over different vegetation cover types and a lag-time relationship is established based on preceding rainfall. The results indicate that during the major drought event of spring 2010, Evergreen Forest (EF) experienced severe dry conditions for 48 days fewer than Cropland (CL) and Shrubland (SL). Testing of vegetation response to drought conditions with different lag-time periods since the last rainfall indicated a highest correlation for CL and SL with the 4th lag period (*i.e.*, 64 days) whereas EF exhibited maximum correlation with the 5th lag period (*i.e.*, 80 days). Evergreen Forest, which includes tree crops, appears to act as a green reservoir of water, and is more resistant than CL and SL to drought due to its water retention capacity with deeper roots to tap sub-surface water. Identifying differences in rainfall lag-time relationships among land cover types using a remote sensing-based integrated drought index enables more accurate drought prediction, and can thus assist in the development of more specific drought adaptation strategies.

Keywords: NDVI; NVSWI; drought index; LST; TRMM

1. Introduction

Periods of persistent abnormally dry weather, known as droughts, can produce serious agricultural, ecological, or hydrological imbalances and have severe environmental, social, and economic effects [1]. Impacts depend on the degree of moisture deficiency, duration, and size of affected area [2]. Drought can be monitored either through classical climatic drought indices from station-based meteorological data sets or through modern Remote Sensing (RS) based drought indices.

Generally, RS based indices for droughts can be categorized into four classes. The first deals with spectral properties of soil with an assumption that soil moisture conditions portray significant changes in the spectral reflectance patterns of soil. In the optical wavelength ranges, 0.4–2.5 μm, the spectral reflectance of soil is inversely proportional to its moisture content [3]. For example, based on three spectral bands, the Normalized Multiband Drought Index (NMDI) was recently developed for monitoring soil water content [4]. In the thermal region (3.5–14 μm), a thermal inertia (TI) method has been developed based on an assumed lower diurnal temperature fluctuation in moist soil (high TI). However, applications of these methods are limited to arid regions with bare land or sparse vegetation [5].

On the other hand, vegetation indices (VIs), such as the NDVI (Normalized Difference Vegetation Index), EVI (Enhanced Vegetation Index, and LAI (Leaf Area Index), are used to represent vegetation condition in drought indices, as the state of vegetation in field and tree crops usually indicates the underlying soil moisture content [6]. Examples of VI-based drought indices are, Vegetation Condition Index (VCI) [7], NDVI Anomaly (NDVIA) [8], and Standardized Vegetation Index (SVI) [9]. The VCI is considered to be suitable to monitor agro-droughts and highly correlated with crop yield [7,10], but its application has limitations and its interpretation is complicated as it is only an indirect measure of soil moisture. However, anything that stresses vegetation including insects, disease, and lack of nutrients will be represented by the VCI [11] and may not be highly correlated with *in situ* meteorological drought indices [1].

The third method of measuring surface moisture is based on the difference between the measured surface temperature and typical baseline temperature of a well-watered crop. The index is known as the Crop Water Stress Index (CWSI) and has been applied for monitoring drought over spatio-temporal scales [12,13]. However, use of CWSI with remote sensing based LST is restricted to full canopy conditions so that the surface temperature sensed is equal to canopy temperature. The Evaporative Stress Index (ESI) has been used to quantify actual evapotranspiration that is important in parts of the world with scarce or unreliable rainfall data sets, using thermal imagery from a geostationary satellite [14].

The thermal stress of the land surface has also attracted researchers' interest, resulting in an LST-based Temperature Condition Index (TCI) [15,16], and subsequently researchers found a combination of vegetation and temperature conditions to be a good indicator of soil moisture content, since both VNIR and TIR based drought indices have merits and demerits in terms of utility for drought detection. The LST is a better indicator over sparse canopies or bare lands, whereas VI-based drought estimates are good for drought indication with moderate vegetation canopy cover. Therefore, using the

complimentary information available from TIR and VNIR, a new set of drought indices were developed as unified drought indicators. Generally, VIs exhibit negative correlation with LST [17,18] from the cooling effect of canopy transpiration, however in energy limited ecosystem NDVI indicates a positive correlation with LST [19,20]. In recent decades several indices based on the NDVI-LST relationship such as Vegetation Health Index (VHI), Temperature-Vegetation Drought Index (TVDI) [21], Vegetation Supply Water Index (VSWI) [22,23], and Drought Severity Index (DSI) [24] have been proposed.

Classical climatic drought indices include the Palmer Drought Severity Index (PDSI) [25], Palmer Moisture Anomaly Index (z-index) [25], and Standardized Precipitation Index (SPI) [26]. Among these, SPI has gained more attention due to its simplicity and flexibility to monitor drought at different temporal scales (e.g., 1, 3, 6, 9, 12 and 24 months intervals) with four drought classes (*i.e.*, near normal, moderate, severe and extreme droughts). Although precipitation has a major influence on drought, precipitation records from climate stations are sparse in most areas and the point data cannot be extended far beyond the stations. Until recently, remote sensing based estimation of drought did not include climatic data, but recent advancements in microwave sensors have produced estimations of global climate parameters as an alternative to ground measurements, including rainfall estimation from the "Tropical Rainfall Measurement Mission (TRMM)" [27,28], CPC Morphing Technique (CMOPHR) [29], and Precipitation Estimation from Remotely Sensed Information using Artificial Neural Networks (PERSIANN) [30]. These near-real time satellite based estimates of precipitation lack the historic context and are mostly available for the last 15 years. Therefore, until recently, these data sets could not be used to produce drought indices that require longer term records.

Soil moisture products of the Advanced Microwave Scanning Radiometer (AMSR-E) [31], have given a new direction to remote sensing based drought indices. Based on multi-sensor data sets, including optical, thermal and microwave sensors, a new generation of integrated remote sensing indices has been developed for agro-drought monitoring using NDVI, LST and TRMM rainfall data. Such indices include the Scaled Drought Condition Index (SDCI) [32], a comprehensive index for assessment of agro-drought severity (SADI) [33], the Microwave Integrated Drought Index (MIDI) [31], and the Synthesized Drought Index (SDI) [1] as well as an integrated method to monitor soil moisture anomalies [34] from TCA (Triple Collocation Analysis) [35] based on merging of AMSR-E, ALEXI (Atmosphere-Land Exchange Inverse surface energy balance algorithm) [36] and the NLSM (Noah Land Surface Model) [37]. Also the Global integrated drought monitoring and prediction system (GIDMaPS) provides near real-time drought information based on multiple drought indicators (e.g., SPI [38], SSI [39], and MSDI [40]) and other input data sets [41].

However, in the case of vegetation moisture conditions, there is a time lag between precipitation occurrences and response of vegetation, and this lag time varies according to regional rainfall patterns [42], soil type [43], land cover and vegetation type [44] or crop type. Furthermore, it may possible that the absence of a particular period or event of rainfall can trigger a drought event, since some crops are very sensitive to specified amount of moisture at specific growth stages. Therefore, it is also necessary to understand the rainfall and drought index (based on VI and LST) relationship specific to local land cover types. Because drought monitoring requires data of high temporal resolution, all previous remote sensing studies have used daily orbiting satellites with low spatial resolution such as AVHRR and MODIS (e.g., [1,7,8,13,16,25,43–45]). They have therefore applied drought indices at

whole landscape level, and no study has identified different land cover types for the derivation of drought parameters. In this study, an attempt has been made to retrieve key drought indicators from MODIS, for different vegetation cover types and to identify the lag-time coefficient of rainfall for each vegetation cover type derived from Landsat data, to incorporate in further development of integrated drought indices.

This study has two main objectives; (1) to implement a drought index for retrieval of key drought indicators for different cover types, including the degree of moisture deficiency, drought duration and areal extent of drought in Yunnan Province, Southwest China; and (2) to discover a lag time relationship between rainfall and moisture conditions derived from the drought index.

2. Study Area

The current study is carried out in three districts, namely Dali Bai Autonomous Prefecture, Chuxiong Yi Autonomous Prefecture, and Kunming Municipality, in central Yunnan Province, Southwest China (Figure 1). The study area extends from 24 °6′0″N to 26 °48′0″N and from 97 °42′0″E to 103 °48′36″E. All the analyses have been performed within a rectangular area covering these three districts, as they were the most severely affected by the drought in spring 2010 [46]. The size of the study area is approximately 14,000 km^2 and elevation rises to ~4300 m. In Yunnan Province 94% of the area is mountainous, and the average altitude of agricultural areas ranges from 1000 m (in the southwest) to 2600 m (in the northwest). Situated at the confluence of three geographic regions: the eastern Asia monsoon region, the Tibetan plateau region, and the tropical Indian monsoon region, Yunnan's climate is characterized by a dry monsoon (25% of total precipitation) in winter and humid monsoon in summer (75% of total precipitation), but climate is variable spatially according to altitude and latitude. The mean annual precipitation varies from 600 mm in dry valleys to 1700 mm in the southern and western mountainous areas. Rainfall patterns are controlled by four major circulation patterns (north-eastern Monsoon, south-eastern Monsoon, west-eastern Monsoon and extra-tropical westerlies in north-west). As a result, the onset of the rainy season varies throughout the area and ranges from the end of February to the beginning of June. In central Yunnan, the rainy season typically starts in May [47]. However, drought is a major and frequent natural disaster in southwest China. Over the last three decades more droughts have been observed, which may constitute a long term or permanent climate shift in rainfall patterns. A severe and sustained drought, considered as the worst drought in Yunnan in the last 50 years, was observed in Yunnan province, from winter 2009 to spring 2010 which affected 4.9 million ha of agricultural land [48–50].

3. Data and Methods

3.1. Data and Pre-Processing

The primary data sets used for the study consist of two MODIS products, the NDVI (Normalised Difference Vegetation Index) and LST (Land Surface Temperature), and one TRMM (Tropical Rainfall Measurement Mission) rainfall product. In this study, the NDVI and LST data were used to develop the Vegetation Supply Water Index (VSWI) [22]. The NVSWI was produced to have more

objective indicator than the original VSWI which is only a relative measure. The rainfall data sets were used for cross correlation by covariance analysis between rainfall and the NVSWI time-series.

Figure 1. Location map of study area.

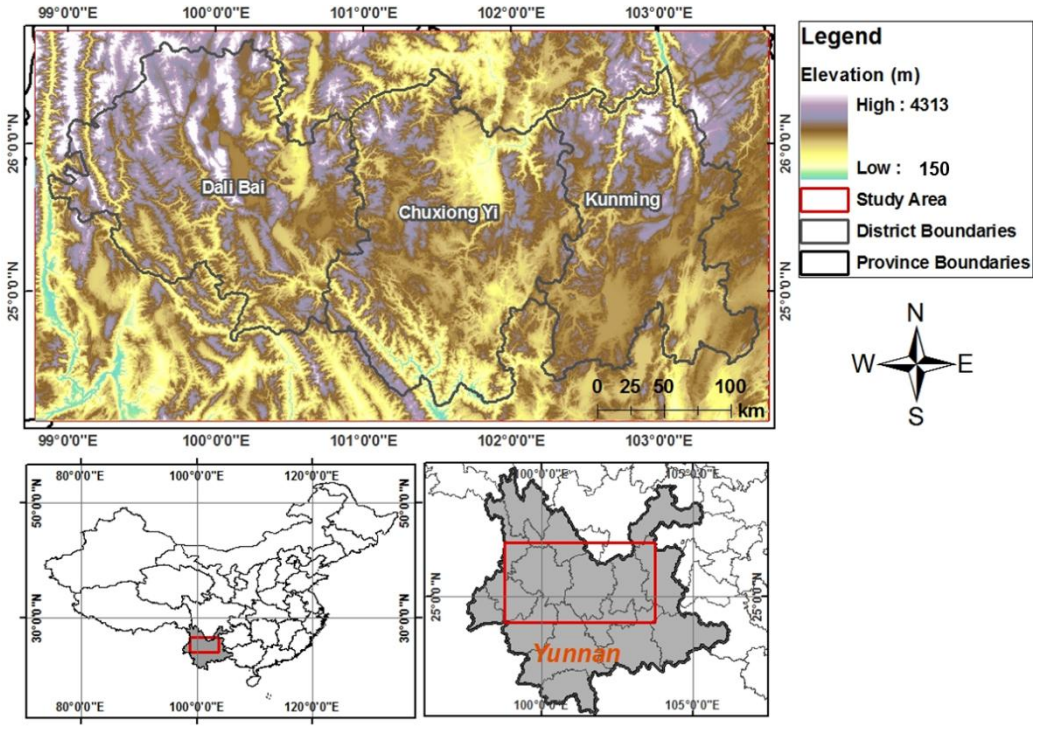

The NDVI shows a high correlation with green biomass and vegetation productivity [51–53]. In the current study, the MODIS NDVI standard product coded as MOD13Q1 (Level 3 Product), for 16-day time intervals and at 250 m spatial resolution, was obtained for the years 2008–2011. These NDVI time series data were smoothed using a state-of-the- art Whittaker filter (the data is freely downloadable from at [54]) [55].

The LST products based on MODIS data have been validated and are considered ready to use in scientific analysis [13,56]. In this research, LST from the Terra MODIS 8-day LST composite with 1 km resolution (MOD11A2, collection v005) was used for the years 2008 to 2011. The 8-day product is based on an average of "two to eight days" LST estimates with clear-sky conditions [57]. To match the NDVI composite temporal resolution, we composited consecutive 8-day LST images to 16-day images. The QA flags accompanying the LST product were used to select good quality pixels. Priority of the QA flags in integer values was; 0, 1, 5, 64, 17, 21, 65, 69, 81, and 85 [58]. If the quality of both 8-day images was equally good then the average was output. Otherwise the better quality pixel was chosen, and if both pixels did not have acceptable quality, the spatial average of neighboring pixels was taken.

The daily rainfall product (3B42) of the TRMM (Tropical Rainfall Measurement Mission) was used as an alternative to station based rainfall measurements. This product extends from 50 ° north to 50 ° south with spatial resolution of 0.25 ° (for more detail: see [59]). The 3B42 product is a daily average, and can be simply converted by multiplying by 24 in order to have accumulated rainfall for the day [30,60,61]. For our analysis daily rainfall was also composited into 16-day accumulated rainfall. Although the use of TRMM rainfall data is well established, before further use of TRMM rainfall data, they were validated and compared with ground based rainfall measurements. Historic (1961–2007) and

recent (2008–2011) monthly rainfall measurements from the Kunming ground station were acquired from the statistical yearbook of China. Similarly, historic records of mean monthly rainfall (1961–1990) were obtained from the Hong Kong Observatory [62] and data from 1991 to 2007 was taken from statistical year books of China [63–79]. These data sets were used for validation of TRMM rainfall measurements and for identification of relatively dry/wet years.

The Land Cover Land Use (LCLU) map of the study area was prepared from two available global LCLU products, the MODIS LCLU at 500 m and GLC2000 LCLU derived from Landsat at 30 m resolution. The GLC2000 LCLU appeared more accurate than MODIS LCLU when validated with Google Earth imagery, but "Urban Areas", which were better mapped in the MODIS product, were mosaicked into the GLC2000 LCLU. Additionally, an omission error in the in GLC2000 "Cropland" class whereby most "Cropland" class, identified at high resolution imagery on Google Earth™, was misclassified as "Grassland", was addressed by merging Grassland into Cropland. The final LCLU map output at 30 m resolution consisting of seven LCLU classes, viz., Built-up Area, Cropland (CL), Shrubland (SL), Deciduous Forest (DF), Evergreen Forest (EF), Mixed Forest (MF), and Water (W), was resampled to 250 m, along with all other datasets (Figure S1).

3.2. Validation of TRMM Rainfall Data

Monthly satellite-based rainfall estimates from TRMM and *in situ* rainfall measurements from the Kunming ground station were compared over the study period of 2007 to 2011, using Deming Regression (DR) [80] analysis on 60 observations within the period (Equation (1)).

$$R_{(TRMM)} = f_{(R_{in-situ})} \quad (1)$$

The correlation coefficient (R) is a good indicator of agreement between two variables. We used DR as opposed to Linear Regression (LR) because DR estimates an unbiased slope by assuming a Gaussian distribution of errors in both x and y data points [81].

Statistical indicators (namely—slope (m), intercept (c), correlation coefficient (R), root mean square error (RMSE), and mean absolute error (MAE), were used to evaluate the satellite based estimation of rainfall against ground station rainfall (Table S1).

3.3. Drought Index: Vegetation Supply Water Index (VSWI)

The VSWI (Equation (2)) is based on the assumption that under normal conditions, with sufficient soil water supply, land surface temperature observed over vegetation will have low values due to cooling effects of evapotranspiration [82] (Figure S2). When vegetation suffers from drought, soil water deficit causes leaf stoma to partly close in order to sustain water in the canopy. As a result, evapotranspiration is reduced and LST increases. The accompanied withering of leaves has negative effect on NDVI which is dependent upon leaf health. Cai *et al.* 2011 [83] applied the same approach to indicate the spatial spread of drought in Yunnan province using a single observation of MODIS-based NDVI and LST on 7 March 2011.

$$VSWI = \frac{NDVI}{LST} \quad (2)$$

In present study, the VSWI used for drought monitoring was modified, as the index gives only values relative to the scene and study area and does not convey real meaning in terms of drought severity. Therefore the VSWI values were normalised over the study period (2008 to 2011), to give NVSWI (Equation (3)) which permits realistic and absolute comparisons within the study period

$$NVSWI = \frac{(VSWI - VSWI_{min})}{(VSWI_{max} - VSWI_{min})} \times 100 \quad (3)$$

where *NVSWI* is Normalized Vegetation Supply Water Index, $VSWI_{min}$ and $VSWI_{max}$ are minimum and maximum value of *VSWI* of the pixel during the period of study, respectively.

The index, with values of 0 to 100, portrays relative drought conditions across the years and between the years, with an *NVSWI* of zero indicating severest drought during the study period and *NVSWI* of 100 indicating wettest conditions. The index values were categorized into five drought classes, namely severe drought (<20), moderate drought (20–40), slight drought (40–60), normal (60–80), and wet (>80). Availability of *in situ* field data would be likely to permit more meaningful class division. An Equal Interval classification was used for categorization of normalized values, because if a normal distribution is assumed, this method is able to indicate extreme high and low values such as exceptionally wet, and severe dry conditions.

3.4. Normalized Rainfall Difference (NRD)

The Normalized Rainfall Difference was calculated based on *in situ* monthly measurement from 2008 to 2011 and mean monthly precipitation recorded by historic records over 47 years (1961–2007).

$$NRD = \frac{(R - R_m)}{(R_{max} - R_{min})} \times 100$$

where *R* is rainfall of corresponding month, R_m is the historic average of rainfall of the month, R_{min} and R_{max} are minimum and maximum monthly rainfall during the period, respectively.

The NRD is assumed to represent the difference in rainfall from the historical average, and its purpose is to indicate relative rainfall deficit rather than identifying a drought event (as indicated through classical drought indices such as SPI) (Figure S3).

3.5. Covariance of Drought Index and Rainfall Time Series

The response of the NVSWI time series to rainfall series with different lag-time scales (0, 16, 32, …, 128 days) for each of LCLU class (*i.e.*, CL, SL and EF) was analyzed using Pearson's cross correlation (PCC) analysis [84]. This was performed up to the 8th lag period corresponding to 16, 32, …, 128 days lag-periods.

In order to assess the robustness of the methodology, the index was also implemented in an additional study area which we conducted in the Koshi River Basin in the Himalayan region (Figure S4), and the results were very similar (Figures S5 and S6). We also used satellite derived monthly SPI (based on GPCP [85] and PERSIANN [30]), after Aghakouchal [38], to verify the same drought event and to draw a comparison between the SPI and NVSWI time series (Figures S3 and S7).

4. Results and Discussions

4.1. LCLU Dynamics

Approximately 95.75% of the area is dominated by three major LCLU types, which are—EF (40.80%), CL (38.26%), and SL (16.69%) (Table 1). The elevation profile of the LCLU classes (Figure 2) indicates CL extends from 600 m to 2700 m with maximum cover around 2000 m, whereas EF ranges from 1200 m to 3700 m with maximum cover around 2200 m. However, SL occupies a comparatively narrow altitudinal range from around 700 m to 2200 m with major cover around 1800 m. It is also notable that natural vegetation is dominated by SL at lower elevations up to 1800 m, which seems to be transitional to EF above 1800 m elevation.

Table 1. Distribution of LCLU classes in the study area.

No.	LCLU Classes	Area (10^3 ha)	Percentage Area
1	Built-up Area	66.35	0.46
2	Cropland	5574.42	38.26
3	Deciduous Forest	10.066	0.07
4	Evergreen Forest	5955.31	40.87
5	Mixed Forest	372.71	2.55
6	Shrubland	2431.90	16.69
7	Water	161.4	1.11
	Total	14571.46	100.00

Figure 2. Elevation profile of the major LCLU classes.

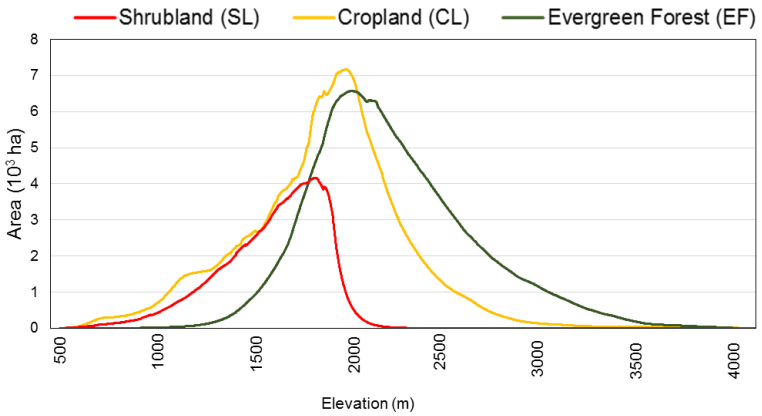

4.2. Validation of TRMM Rainfall with in situ Rainfall

Literature suggests that TRMM rainfall measures have potential to substitute for ground based observations [86–88]. In this study, TRMM estimates of rainfall have been used as an alternative to *in situ* observations, and a comparison with ground station data (Figure 3) indicates a very similar magnitude and temporal pattern over the study period, with a correlation coefficient of 0.97 (Figure 4). The relationship is statistically significant (based on F-statistics and t-statistics with p values less than 0.01) such that TRMM estimates explain 94% of the variability in observed rainfall estimates at the ground station (Table S1). In Figure 4 the majority of the observations lie close to the 1:1 line

when the amount of rainfall is less than 100 mm. For 100 mm to 150 mm the TRMM rainfall gives slight underestimates but for higher rainfall values (>150 mm) TRMM rainfall highly underestimates and the RMSE is increased. However, the pattern of both measurements are similar, as indicated by the high correlations and visual patterns in Figure 3. The underestimation of TRMM rainfall in summer is in not negligible in absolute terms. However, as we are interested in relative deficiency of rainfall, we can assume this is not biasing the output. The analysis concludes that RS based rainfall measures can be used as an alternative to *in situ* rainfall estimates for this study, although the result may vary in other geographical regions.

Figure 3. Comparison of TRMM and *in situ* rainfall measurements.

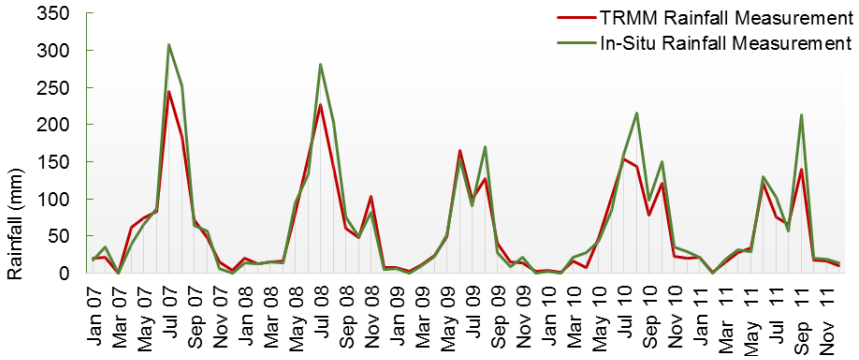

Figure 4. Regression analysis between monthly TRMM and *in situ* rainfall measurements.

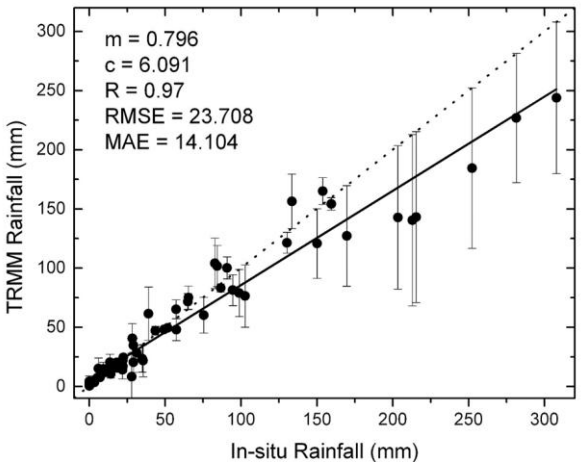

4.3. Drought Identification from Rainfall Records

Figure 5 shows the monthly deviation of rainfall from a 47-year historic average and suggests a shortage of rainfall in the study area in 2009, and that the year 2009, within the 4-year period, is the most seriously affected. Spring droughts in the region have serious repercussions on livelihoods as they come at the start of the growing season, and these are dependent on rainfall from November to February. It can be seen that November 2009 to February 2010 had a significant deficit (red circle) compared to normal years. The impact of this drought spell is evident in the moisture index derived from RS data sets (Figure 6) where the March to June growing season of 2010 was under Severe Dry, *i.e.*, drought conditions. The accumulated winter season rainfall in 2008–2009, 2009–2010, and

2010–2011 is recorded as 95.2, 25.7 and 86.2 mm, respectively (whereas the accumulated 47-year winter rainfall average is 62.98 mm). The higher rainfall in November 2008 and December to January of 2010–2011 is reflected in increased vegetation moisture conditions in the subsequent spring seasons of 2009 and 2011 (Figure 6). Thus, we may deduce that rainfall in the winter season is critical for vegetation moisture conditions in the following spring and early summer season (May–June), which corresponds to the main growing season.

Figure 5. Normalized difference of monthly rainfall (2008–2011) from 47-year mean monthly rainfall (1961–2007).

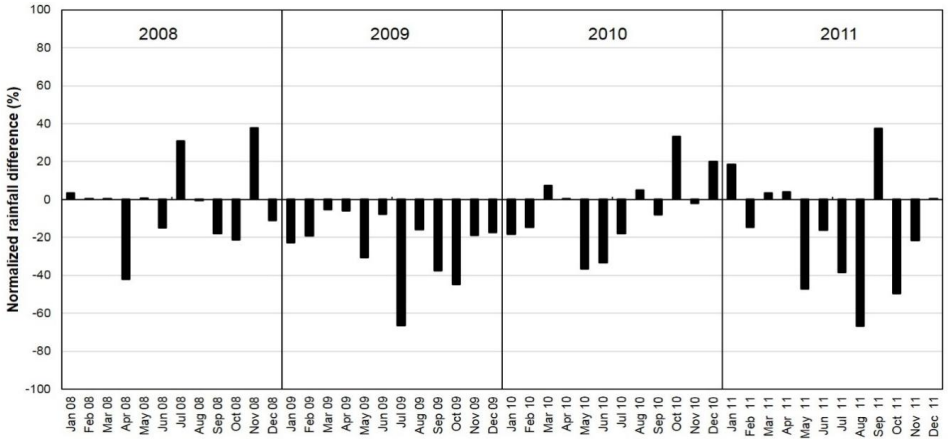

Figure 6. Year to year spatial patterns of moisture conditions from NVSWI.

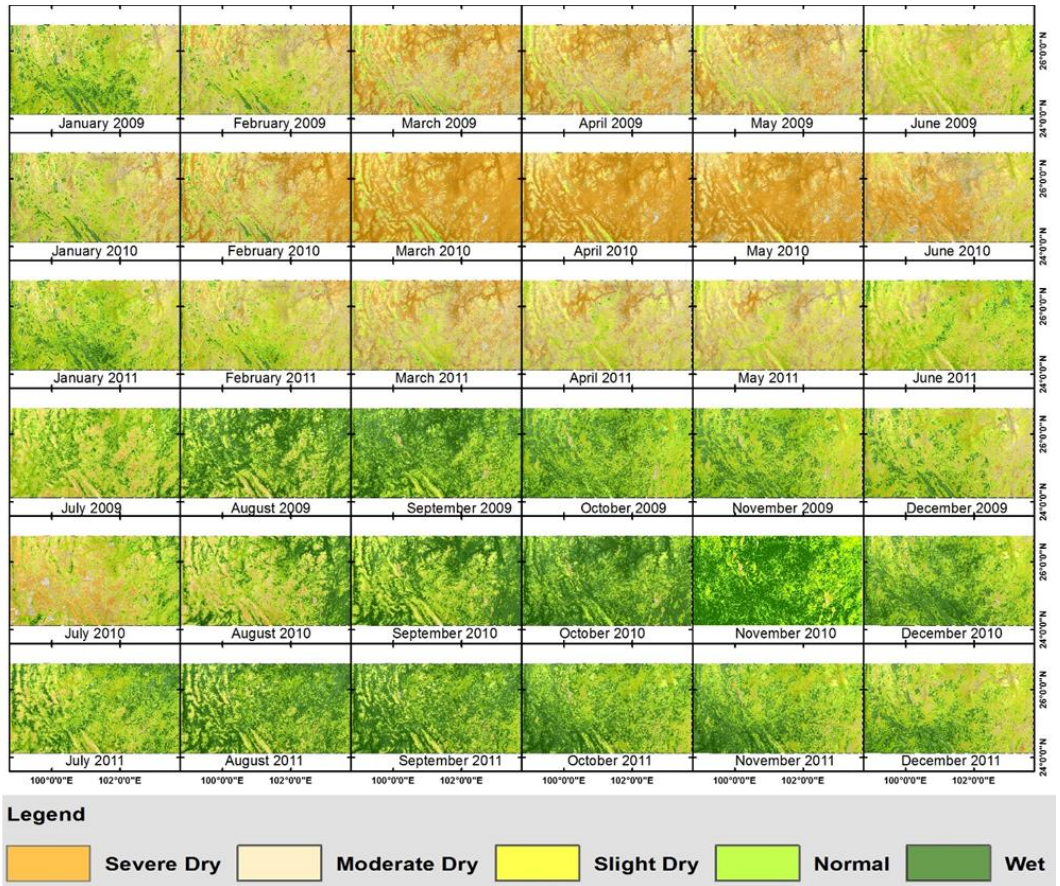

4.4. Spatio-Temporal Patterns of Drought

Time series of spatially averaged NVSWI over the major LULC classes in the study show annual and seasonal cycles of moisture conditions (Figure 7). Moisture contents reach maximum values during July, August, and September, whereas minimum values are observed around March and April. It is discernable, wet season usually begins in June and lasts till the end of November. By December, vegetation starts to get drier and reaches maximum dryness in March-April, and dry season ends in May. A time series graph of the index clearly indicates abnormally dry conditions in the 2009–2010 dry season, which is visible (*i.e.* Slight Dry Range) until August and the wet season seems to be prolonged into November–December of 2010 (Figure 7). The temporal span of drought also indicates March-May as the driest time during the drought spell of 2010. Although EF experienced delayed dryness during that drought period (Figure 7), by March-to-May the drought had become homogenous across the land cover types with approximately 80% of the area under severe dry conditions (Figure 6).

Figure 7. Spatially averaged NVSWI time-series of the LCLU classes.

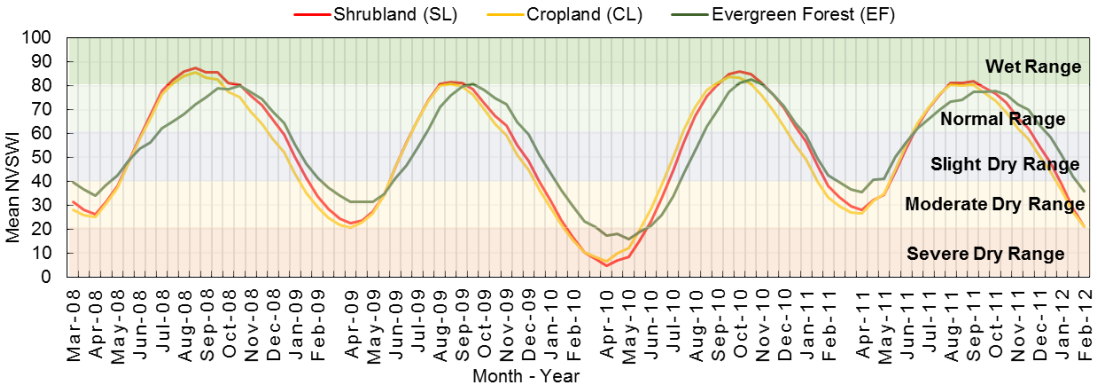

Degree of moisture deficiency: The effect of winter drought on vegetation is observed to start in early spring 2010, become severe in April and extend until the end of August. During this time, CL and SL followed similar patterns of moisture conditions but EF portrayed a distinct signature of moisture conditions as it remained relatively stable in both dry and wet seasons (Figure 7). Notably, in spring 2010 CL and SL experienced severe dry conditions while EF remained resistant to them. In terms of moisture deficiency severity, EF indicated the least severe dry conditions with approximately 70%, and 58% less than SL and CL respectively (and a delay of ~30 days to reach severe dry conditions).

Drought duration: By overlaying the LCLU onto the NVSWI images, the amount of time in each year that each cover type spent under different moisture conditions can be seen (Figure 8). EF spent the fewest days under Severe Dry conditions and most of the time it remained under normal conditions. CL and SL spent more time than EF under Severe Dry and Moderate Dry conditions. In addition to the difference in the number of days, EF exhibited almost 32 days delay in drought onset in comparison to CL and SL (Figure 7). Thus, EF exhibited the greatest resilience to severe drought, which suggests it can adapt to drought through leaf stomata closure to reduce water loss from evapotranspiration, and a deeper root system [89,90]. CL and SL suffered approximately 30 days more drought than EF (Figure 8). On the other hand, in the severe drought spell of 2010, EF experienced 48 days more in Moderate Dry conditions than SL, and 16 days more than CL. The area representing

Normal conditions in Figure 8 was much lower during the 2009–2010 drought spell, and the area representing Moderate Dry and Severe Dry conditions, higher than in other years. Much of the time that the vegetation types spend under Normal conditions has been shifted to Moderate and Severe Dry conditions. In comparison to CL and SL, EF spent considerably longer time (~4 weeks more than CL and SL) in Normal conditions and spent less time (~2 weeks less than CL and SL) in Wet conditions (Figure 8). From Figures 6–8, it can be deduced that the amount of time spent by CL, SL and EF under wet conditions is similar but the wet season shifted later in the drought year of 2010. Evidence from TRMM data (Figure 6) suggests that the image-derived drought was not merely due to late sowing and late harvesting of crops, but was a rainfall-induced drought, *i.e.*, a temporary shift in growing season. Moisture was lowest from April to May 2010 was lowest due to spring drought, whereas very high moisture conditions are observed from October to November 2010 due to exceptionally high rainfall in late summer and early winter (Figures 5, 6 and 9). Thus, the shift in vegetation calendar is primarily driven by changes in the rainfall pattern. Zhang *et al.* [91] also observed this temporal shift in primary productivity during the 2010 drought event in south-western China, and found that the GPP and NPP were lowest from 2000 to 2010.

Figure 8. Distribution of number of days of the LCLU classes under different moisture conditions, based on overlay of LCLU map on NVSWI image.

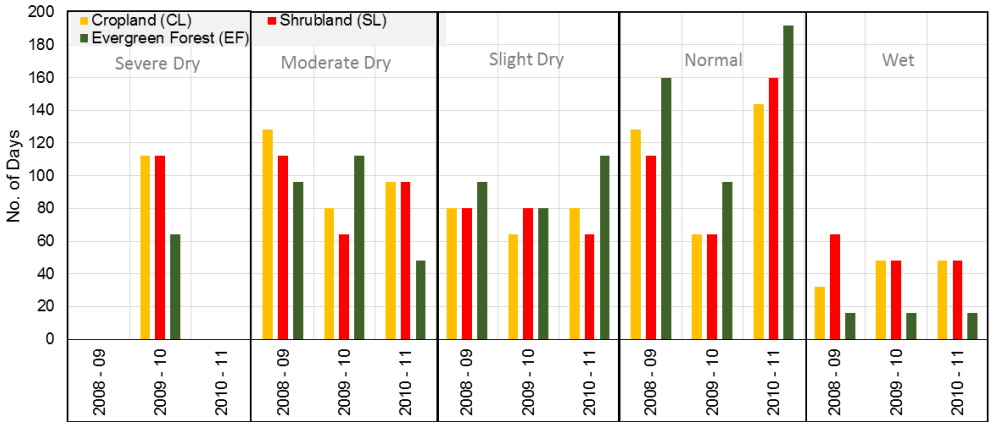

Figure 9. Spatially averaged NVSWI corresponding to the LCLU classes and spatially mean rainfall patterns across the time. Mean rainfall and Mean Rainfall (Moving Average by 5) are plotted on secondary Y-axis.

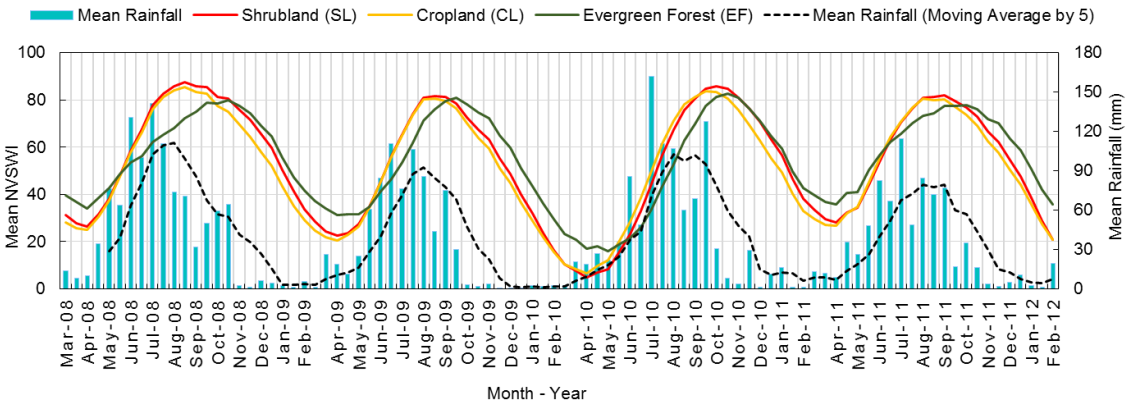

4.5. Rainfall and Vegetation Moisture Conditions

To assess the relationship between rainfall and vegetation moisture conditions implied by the drought index, PCC was performed between time series of NVSWI and rainfall across the LCLU classes over the entire period of analysis (2008–2011) (Table 2 and Figure 10). Rainfall lag times (16, 32, 48, …, 128) were incorporated in the analysis to identify the drought resilience of the vegetation types in the area. Table 2 shows that the correlation coefficients varied significantly by the lag time (as indicated in Figure 10 also) and by vegetation type. CL and SL indicated highest correlations (R = 0.80 and 0.82, respectively) with the 4th lag period (~64 days earlier) of rainfall, whereas, EF exhibited strongest correlation coefficients (R = 0.79) with the 5th lag period (~80 days earlier) of rainfall. It is notable that the correlation coefficient for EF is considerably lower than that for CL and SL up to the 4th lag period, while during the 5th to 8th lag period it obtained a higher correlation coefficient. This suggests that EF can retain moisture from earlier rainfall events. EF is clearly more resilient to drought conditions and least affected by the rainfall deficit acting as a green reservoir of water. However it should be noted that the time lag between precipitation occurrence and response of vegetation may be particular to this study and may vary in other parts of the globe. For example, lag time of one to two months is reported in natural ecosystems of South Africa [92], and 24 to 64 days is observed in Central and South West Asian Region [84].

Figure 10. Plot of correlation between spatially averaged NVSWI of the LCLU classes and rainfall time series with different lag times.

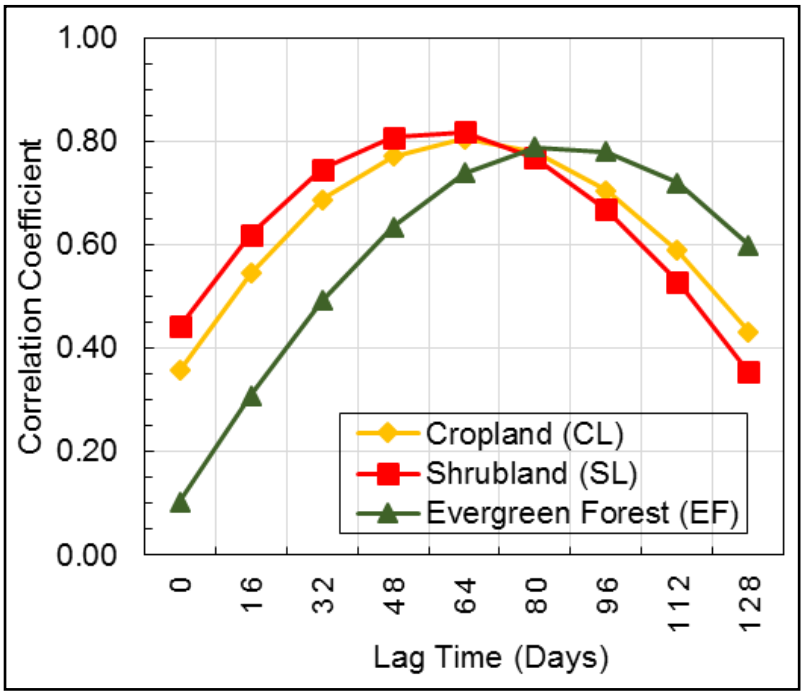

When compared with a time series plot of the SPI [38] which is based on *in situ* rainfall data, NVSWI which indicates conditions across the whole landscape showed a lag time of about two months while the drought severity observed by both indices was similar. The SPI indicated maximum severity in February while NSVWI indicated severe effects on vegetation across the study area in April. The

time under severe dry conditions, as characterized by the SPI was approximately 60 days (20 January to 22 March) and for the NVSWI, 110 days (20 February to 10 June) (Figures S3 and S7).

Table 2 Correlation values of the LCLU classes corresponding to lag time scale of rainfall.

Rainfall Lag Time Scale (Days)	Cropland	Shrubland	Evergreen Forest
0	0.36	0.44	0.10
16	0.54	0.62	0.31
32	0.69	0.75	0.49
48	0.77	0.81	0.63
64	**0.80**	**0.82**	0.74
80	0.78	0.77	**0.79**
96	0.70	0.67	0.78
112	0.59	0.53	0.72
128	0.43	0.35	0.60

Since our index uses temporally normalized data, it was possible to precisely discriminate between degrees of moisture stress across the time scale. Such an approach is more useful for understanding detailed drought conditions across different land use/land cover types at local scale, in comparison to conventional drought indices which are mainly used for regional and global studies. The current approach can therefore provide, important information for development of practical adaptation strategies. The current work is focused on characterization of drought conditions during an extreme event and its impacts on local ecosystems. The main limitations are that the time lag relationships are study area specific, and the index may not be appropriate for sparse vegetation canopies due to the influence of background soil reflectance on the NDVI as well as on LST.

5. Conclusion

In this study, the applicability of remote sensing data products for characterizing severe drought across the landscape, as opposed to classical drought indices based on fixed rainfall data, is assessed. The results demonstrate that the empirical NDVI-LST relationship can be effectively exploited as an indicator of spatial temporal characteristics of water stress conditions, and the high correlation (R = 0.97) between Tropical Rainfall Measuring Mission (TRMM) images and *in situ* rainfall data recommends the use of image-based rainfall estimates in integrated drought indices. The effect of drought on the major vegetation communities (Cropland, Shrubland, and Evergreen Forest) was characterized using a remote sensing approach in terms of on-set, length, and severity of drought. It was found that Evergreen Forest was the least affected by the severe drought spell of 2009–2010, as it was less dry and spent approximately 32 days less than the other vegetation types under Severe Dry condition. Rather, it spent a longer time (~32–48 days) in Moderate Dry conditions. Furthermore, the highest correlation (R = 0.79) of the image-derived moisture conditions for Evergreen Forest with two and a half month's earlier rainfall indicates higher resilience to drought, of Evergreen Forest than Cropland and Shrubland, which showed highest correlations (R = 0.80 and 0.82) with two months earlier rainfall. Thus, Cropland and Shrubland can sustain moisture from only two months earlier rainfall and this dependence on earlier rainfall further decreases with increase in lag time after the two

months. In summary, Evergreen Forest acts as a green reservoir of water, and is more resilient to drought due to its water storage ability and deeper roots to approach sub-surface water resources. The impacts of a spring 2010 drought in Yunnan, China, were visible until the end of August, and exceptionally extended wet conditions into October and November as a result of late summer rainfall were also discernible. Drought frequency has increased in Yunnan, and is projected to become more severe in the 21st century [93]. Severe drought resulting from a long and extended winter dry season can delay spring germination, and also reduce summer productivity by reducing the length of growing season. Using the predicted lag time relationships observed in this study, remote sensing datasets can provide several months of advanced warning of such droughts, across the whole landscape, and with adequate spatial resolution of 250 m, to permit stakeholders to distinguish between the land cover types affected. These lag time relationships provide a way forward for remote sensing-based integrated drought monitoring, as well as predictions of drought specific to cover type.

Acknowledgments

This work is primarily done through the Ph.D. fellowship provided by the Research Grant Council-Hong Kong and RGC grant No. G-RUYX and PolyU5225/13E. Authors would also like to acknowledge the support drawn from The HICAP and SERVIR Himalaya programs of ICIMOD, and CGIAR Research Program 6 on Forests, Trees and Agroforestry. The authors benefitted from discussions and comments from Robert Zoomer (CMES), MSR Murthy (ICIMOD), Muhammad Imran Shahzad, Muhammad Bilal, Syed Muhammad Irteza and Majid Nazir (PolyU). The authors sincerely thank the anonymous reviewers for their very helpful comments and suggestions. The views expressed are those of the author's and do not necessarily reflect that of the organizations mentioned above.

Author Contributions

The idea was conceived by Sawaid Abbas and Janet E. Nichol, performed by Sawaid Abbas and Faisal M. Qamer, written by Sawaid Abbas and Janet E. Nichol, and analyzed by Jianchu Xu.

Conflicts of Interest

The authors declare no conflict of interest

References and Notes

1. Du, L.; Tian, Q.; Yu, T.; Meng, Q.; Jancso, T.; Udvardy, P.; Huang, Y. A comprehensive drought monitoring method integrating MODIS and TRMM data. *Int. J. Appl. Earth Obs. Geoinf.* **2013**, *23*, 245–253.
2. Wilhite, D.A.; Glantz, M.H. Understanding: The drought phenomenon: The role of definitions. *Water Int.* **1985**, *10*, 111–120
3. Bowers, S.A.; Hanks, R.J. Reflection of radiant energy from soils. *Soil Sci.* **1965**, *100*, 130–138.
4. Wang, L.; Qu, J. Satellite remote sensing applications for surface soil moisture monitoring: A review. *Front. Earth Sci. China* **2009**, *3*, 237–247.

5. Xue, H.; Ni, S. Progress in the study on monitoring of soil moisture with thermal infrared remote sensing. *Agric. Res. Arid Areas* **2006**, *24*, 168–172.
6. Mao, K.; Ma, Y.; Xia, L.; Tang, H.; Han, L. The monitoring analysis for the drought in China by using an improved MPI method. *J. Integr. Agric.* **2012**, *11*, 1048–1058.
7. Kogan, F. World droughts in the new millennium from AVHRR-based vegetation health indices. *Eos. Trans. Am. Geophys. Union* **2002**, *83*, 557–563.
8. Anyamba, A.; Tucker, C.J.; Eastman, J.R. NDVI anomaly patterns over Africa during the 1997/98 ENSO warm event. *Int. J. Remote Sens.* **2001**, *22*, 1847–1859.
9. Peters, A.J.; Waltershea, E.A.; Ji, L.; Vliia, A.; Hayes, M.; Svoboda, M.D. Drought monitoring with NDVI-based standardized vegetation index. **2002**, *68*, 71–75.
10. Salazar, L.; Kogan, F.; Roytman, L. Using vegetation health indices and partial least squares method for estimation of corn yield. *Int. J. Remote Sens.* **2008**, *29*, 175–189.
11. Vicente-Serrano, S.M. Evaluating the impact of drought using remote sensing in a Mediterranean, semi-arid region. *Nat. Hazards* **2006**, *40*, 173–208.
12. Jackson, R.D.; Idso, S.B.; Reginato, R.J.; Pinter, P.J. Temperature as a crop water stress indicator. *Water Resour. Res.* **1981**, *17*, 1133–1138.
13. Son, N.T.; Chen, C.F.; Chen, C.R.; Chang, L.Y.; Minh, V.Q. Monitoring agricultural drought in the Lower Mekong Basin using MODIS NDVI and land surface temperature data. *Int. J. Appl. Earth Obs. Geoinf.* **2012**, *18*, 417–427.
14. Anderson, M.C.; Hain, C.; Wardlow, B.; Pimstein, A.; Mecikalski, J.R.; Kustas, W.P. Evaluation of drought indices based on thermal remote sensing of evapotranspiration over the Continental United States. *J. Clim.* **2011**, *24*, 2025–2044.
15. Kogan, F.N. Global drought watch from space. *Bull. Amer. Meteorol. Soc.* **1997**, *78*, 621–636.
16. Jain, S.K.; Keshri, R.; Goswami, A.; Sarkar, A.; Chaudhry, A. Identification of drought-vulnerable areas using NOAA AVHRR data. *Int. J. Remote Sens.* **2009**, *30*, 2653–2668.
17. Goetz, S.J. Multi-sensor analysis of NDVI, surface temperature and biophysical variables at a mixed grassland site. *Int. J. Remote Sens.* **1997**, *18*, 71–94.
18. Nemani, R.; Pierce, L.; Running, S. Developing satellite-derived estimates of surface moisture status. *J. Appl. Meterorol.* **1993**, *32*, 548–557.
19. Karnieli, A.; Bayasgalan, M.; Bayarjargal, Y.; Agam, N.; Khudulmur, S.; Tucker, C.J. Comments on the use of the Vegetation Health Index over Mongolia. *Int. J. Remote Sens.* **2006**, *27*, 2017–2024.
20. Karnieli, A.; Agam, N.; Pinker, R.T.; Anderson, M.; Imhoff, M.L.; Gutman, G.G.; Panov, N.; Goldberg, A. Use of NDVI and land surface temperature for drought assessment: Merits and limitations. *J. Clim.* **2010**, *23*, 618–633.
21. Sandholt, I.; Rasmussen, K.; Andersen, J. A simple interpretation of the surface temperature/vegetation index space for assessment of surface moisture status. *Remote Sens. Environ.* **2002**, *79*, 213–224.
22. Carlson, T.N.; Perry, E.M.; Schmugge, T.J. Remote estimation of soil moisture availability and fractional vegetation cover for agricultural fields. *Agric. For. Meteorol.* **1990**, *52*, 45–69.

23. Carlson, T.N.; Gillies, R.R.; Perry, E.M. A method to make use of thermal infrared temperature and NDVI measurements to infer surface soil water content and fractional vegetation cover. *Remote Sens. Rev.* **1994**, *9*, 161–173.
24. Mu, Q.; Zhao, M.; Kimball, J.S.; McDowell, N.G.; Running, S.W. A remotely sensed global terrestrial drought severity index. *Bull. Am. Meteorol. Soc.* **2013**, *94*, 83–98.
25. Palmer, W. *Metreological Drought*; Weather Bureau, US Department of Commerce: Washington, DC, USA, 1965.
26. McKee, T.B.; Doesken, N.J.; Kleist, J. Drought Monitoring with Multiple Time Scales. In Proceedings of the 1995 Conference on Applied Climatology, Dallas, TX, USA, 15–20 January, 1995; American Meteorological Society: Boston, MA, USA, 1995; pp. 233–236.
27. Moffitt, C.B.; Hossain, F.; Adler, R.F.; Yilmaz, K.K.; Pierce, H.F. Validation of a TRMM-based global flood detection system in Bangladesh. *Int. J. Appl. Earth Obs. Geoinf.* **2011**, *13*, 165–177.
28. Almazroui, M. Calibration of TRMM rainfall climatology over Saudi Arabia during 1998–2009. *Atmos. Res.* **2011**, *99*, 400–414.
29. Joyce, R.J.; Janowiak, J.E.; Arkin, P.A.; Xie, P. CMORPH: A method that produces global precipitation estimates from passive microwave and infrared data at high spatial and temporal resolution. *J. Hydrometeor*. **2004**, *5*, 487–503.
30. Huffman, G.J.; Bolvin, D.T.; Nelkin, E.J.; Wolff, D.B.; Adler, R.F.; Gu, G.; Hong, Y.; Bowman, K.P.; Stocker, E.F. The TRMM Multisatellite Precipitation Analysis (TMPA): Quasi-global, multiyear, combined-sensor precipitation estimates at fine scales. *J. Hydrometeorol.* **2007**, *8*, 38–55.
31. Zhang, A.; Jia, G. Monitoring meteorological drought in semiarid regions using multi-sensor microwave remote sensing data. *Remote Sens. Environ.* **2013**, *134*, 12–23.
32. Rhee, J.; Im, J.; Carbone, G.J. Monitoring agricultural drought for arid and humid regions using multi-sensor remote sensing data. *Remote Sens. Environ.* **2010**, *114*, 2875–2887.
33. Gao, M.; Qin, Z.; Zhang, H.; Lu, L.; Zhou, X.; Yang, X. Remote sensing of agro-droughts in Guangdong Province of China using MODIS satellite data. *Sensors* **2008**, *8*, 4687–4708.
34. Anderson, W.B.; Zaitchik, B.F.; Hain, C.R.; Anderson, M.C.; Yilmaz, M.T.; Mecikalski, J.; Schultz, L. Towards an integrated soil moisture drought monitor for East Africa. *Hydrol. Earth Syst. Sci.* **2012**, *16*, 2893–2913.
35. Zwieback, S.; Scipal, K.; Dorigo, W.; Wagner, W. Structural and statistical properties of the collocation technique for error characterization. *Nonlinear Process. Geophys.* **2012**, *19*, 69–80.
36. Anderson, M.C.; Kustas, W.P.; Norman, J.M.; Hain, C.R.; Mecikalski, J.R.; Schultz, L.; González-Dugo, M.P.; Cammalleri, C.; d'Urso, G.; Pimstein, A.; *et al.* Mapping daily evapotranspiration at field to global scales using geostationary and polar orbiting satellite imagery. *Hydrol. Earth Syst. Sci. Discuss.* **2010**, *7*, 5957–5990.
37. Ek, M.B. Implementation of Noah land surface model advances in the National Centers for Environmental Prediction operational mesoscale Eta model. *J. Geophys. Res.* **2003**, *108*, 8851.
38. AghaKouchak, A.; Nakhjiri, N. A near real-time satellite-based global drought climate data record. *Environ. Res. Lett.* **2012**, *7*, 044037.

39. Aghakouchak, A. A baseline probabilistic drought forecasting framework using Standardized Soil Moisture Index: Application to the 2012 United States drought. *Hydrol. Earth Syst. Sci. Discuss.* **2014**, *11*, 1947–1966.
40. Hao, Z.; AghaKouchak, A. Multivariate Standardized Drought Index: A parametric multi-index model. *Adv. Water Resour.* **2013**, *57*, 12–18.
41. Hao, Z.; AghaKouchak, A.; Nakhjiri, N.; Farahmand, A. Global integrated drought monitoring and prediction system. *Sci. Data* **2014**, *1*, 1–10.
42. Nicholson, S.E.; Farrar, T.J. The influence of soil type on the relationships between NDVI, rainfall, and soil moisture in semiarid Botswana. I. NDVI response to rainfall. *Remote Sens. Environ.* **1994**, *50*, 107–120.
43. Ji, L.; Peters, A.J. Assessing vegetation response to drought in the northern Great Plains using vegetation and drought indices. *Remote Sens. Environ.* **2003**, *87*, 85–98.
44. Wan, Z.; Wang, P.; Li, X. Using MODIS Land Surface Temperature and Normalized Difference Vegetation Index products for monitoring drought in the southern Great Plains, USA. *Int. J. Remote Sens.* **2004**, *25*, 61–72.
45. Bayarjargal, Y.; Karnieli, A.; Bayasgalan, M.; Khudulmur, S.; Gandush, C.; Tucker, C. A comparative study of NOAA-AVHRR derived drought indices using change vector analysis. *Remote Sens. Environ.* **2006**, *105*, 9–22.
46. Qiu, J. China drought highlights future climate threats Shake-up for fusion team. *Nature* **2010**, *465*, 142–143.
47. Thomas, A. The onset of the rainy season in Yunnan province, PR China and its significance for agricultural operations. *Int. J. Biometeorol*. **1993**, *37*, 170–176.
48. Liu, J.; Tan, X.; J, W.; Ma, J.; Zhang, N. Comparative analysis between the 2010 severe drought in Southwest China and typical drought disasters. *China Water Resour*. **2011**, *9*, 17–20.
49. Li, Q.; Yan, N.; Zhang, F.; Chang, S.; Wu, B. Drought monitoring and its impacts assessment in southwest China using remote sensing in the spring of 2010. *Acta Geophys.* **2010**, *65*, 71–80.
50. Wang, W.; Wang, W.; Li, J.; Wu, H.; Xu, C.; Liu, T. The impact of sustained drought on vegetation ecosystem in Southwest China based on remote sensing. *Procedia Environ. Sci.* **2010**, *2*, 1679–1691.
51. Pettorelli, N.; Vik, J.O.; Mysterud, A.; Gaillard, J.-M.; Tucker, C.J.; Stenseth, N.C. Using the satellite-derived NDVI to assess ecological responses to environmental change. *Trends Ecol. Evol.* **2005**, *20*, 503–510.
52. Huete, A; Didan, K.; Miura, T.; Rodriguez, E. .; Gao, X.; Ferreira, L. Overview of the radiometric and biophysical performance of the MODIS vegetation indices. *Remote Sens. Environ.* **2002**, *83*, 195–213.
53. Thein, T.R.; Watson, F.G.R.; Cornish, S.S.; Anderson, T.N.; Newman, W.B.; Lockwood, R.E. Vegetation dynamics of Yellowstone's grazing system. *Terrest. Ecol.* **2008**, *3*, 113–133.
54. University of Natural Resources and Life Sciences, Vienna. Available online: http://ivfl-info.boku.ac.at/ (accessed 15 September 2013).
55. Vuolo, F.; Mattiuzzi, M.; Klisch, A.; Atzberger, C. Data service platform for MODIS vegetation indices time series processing at BOKU Vienna: Current status and future perspectives. *Proc. SPIE* **2012**, doi:10.1117/12.974857.

56. Wan, Z. New refinements and validation of the MODIS Land-Surface Temperature/Emissivity products. *Remote Sens. Environ.* **2008**, *112*, 59–74.
57. Zhou, L.; Tian, Y.; Baidya Roy, S.; Dai, Y.; Chen, H. Diurnal and seasonal variations of wind farm impacts on land surface temperature over western Texas. *Clim. Dyn.* **2013**, *41*, 307–326.
58. Neteler, M. Estimating daily land surface temperatures in mountainous environments by reconstructed MODIS LST data. *Remote Sens.* **2010**, *2*, 333–351.
59. Index of /data/TRMM/Gridded/3B42_V7/. Available online: ftp://disc2.nascom.nasa.gov/data/TRMM/Gridded/3B42_V7/ (accessed on 20 September 2013)
60. Immerzeel, W.W.; Droogers, P.; de Jong, S.M.; Bierkens, M.F.P. Large-scale monitoring of snow cover and runoff simulation in Himalayan river basins using remote sensing. *Remote Sens. Environ.* **2009**, *113*, 40–49.
61. Ward, E.; Buytaert, W.; Peaver, L.; Wheater, H. Evaluation of precipitation products over complex mountainous terrain: A water resources perspective. *Adv. Water Resour.* **2011**, *34*, 1222–1231.
62. The Hong Kong Observatory. The Government of Hong Kong Special Administrative Region. Available online: http://www.hko.gov.hk/wxinfo/climat/world/eng/asia/china/kunming_e.htm (accessed on 30 September 2013).
63. China National Bureau of Statistics. *Statistical Yearbook of China 1991*; Economic Information & Agency, China Statistics Press: Beijing, China, 1991. (In Chinese)
64. China National Bureau of Statistics. *Statistical Yearbook of China 1992*; Economic Information & Agency, China Statistics Press: Beijing, China, 1992. (In Chinese)
65. China National Bureau of Statistics. *Statistical Yearbook of China 1993*; Economic Information & Agency, China Statistics Press: Beijing, China, 1993. (In Chinese)
66. China National Bureau of Statistics. *Statistical Yearbook of China 1994*; Economic Information & Agency, China Statistics Press: Beijing, China, 1994. (In Chinese)
67. China National Bureau of Statistics. *Statistical Yearbook of China 1995*; Economic Information & Agency, China Statistics Press: Beijing, China, 1995. (In Chinese)
68. China National Bureau of Statistics. *Statistical Yearbook of China 1996*; Economic Information & Agency, China Statistics Press: Beijing, China, 1996. (In Chinese)
69. China National Bureau of Statistics. *Statistical Yearbook of China 1997*; Economic Information & Agency, China Statistics Press: Beijing, China, 1997. (In Chinese)
70. China National Bureau of Statistics. *Statistical Yearbook of China 1998*; Economic Information & Agency, China Statistics Press: Beijing, China, 1998. (In Chinese)
71. China National Bureau of Statistics. *Statistical Yearbook of China 1999*; Economic Information & Agency, China Statistics Press: Beijing, China, 1999. (In Chinese)
72. China National Bureau of Statistics. *Statistical Yearbook of China 2000*; Economic Information & Agency, China Statistics Press: Beijing, China, 2000. (In Chinese)
73. China National Bureau of Statistics. *Statistical Yearbook of China 2001*; Economic Information & Agency, China Statistics Press: Beijing, China, 2001. (In Chinese)
74. China National Bureau of Statistics. *Statistical Yearbook of China 2002*; Economic Information & Agency, China Statistics Press: Beijing, China, 2002. (In Chinese)

75. China National Bureau of Statistics. *Statistical Yearbook of China 2003*; Economic Information & Agency, China Statistics Press: Beijing, China, 2003. (In Chinese)
76. China National Bureau of Statistics. *Statistical Yearbook of China 2004*; Economic Information & Agency, China Statistics Press: Beijing, China, 2004. (In Chinese)
77. China National Bureau of Statistics. *Statistical Yearbook of China 2005*; Economic Information & Agency, China Statistics Press: Beijing, China, 2005. (In Chinese)
78. China National Bureau of Statistics. *Statistical Yearbook of China 2006*; Economic Information & Agency, China Statistics Press: Beijing, China, 2006. (In Chinese)
79. China National Bureau of Statistics. *Statistical Yearbook of China 2007*; Economic Information & Agency, China Statistics Press: Beijing, China, 2007. (In Chinese)
80. Deming, W.E. *Statistical Adjustment of Data*; Dover Publications: New York, NY, USA, 1943.
81. Linnet, K. Evaluation of regression procedures for methods comparison studies. *Clin. Chem.* **1993**, *39*, 424–32.
82. Bonan, G.B. Forests and climate change: Forcings, feedbacks, and the climate benefits of forests. *Science* **2008**, *320*, 1444–1449.
83. Cai, G.; Du, M.; Liu, Y. Regional Drought Monitoring and Analysing Using MODIS Data: A Case Study in Yunnan Province. In *Computer and Computing Technologies in Agriculture IV*; Springer: Heidelberg, Germany, 2011; pp. 243–251.
84. Shahabfar, A.; Ghulam, A.; Conrad, C. Understanding hydrological repartitioning and shifts in drought regimes in Central and South-West Asia using MODIS derived perpendicular drought index and TRMM data. *IEEE J. Select. Topics Appl. Earth Observ. Remote Sens.* **2013**, *7*, 1–11.
85. Adler, R.F.; Huffman, G.J.; Chang, A.; Ferraro, R.; Xie, P.; Janowiak, J.; Rudolf, B.; Schneider, U.; Curtis, S.; Bolvin, D.; *et al.* The Version-2 Global Precipitation Climatology Project (GPCP) monthly precipitation analysis (1979–Present). *J. Hydrometeor.* **2003**, *4*, 1147–1167.
86. Barros, A.P.; Joshi, M.; Putkonen, J.; Burbank, D.W. A study of the 1999 monsoon rainfall in a mountainous region in central Nepal using TRMM products and rain gauge observations. *Geophys. Res. Lett.* **2000**, *27*, 3683–3686.
87. Duncan, J.M.A.; Biggs, E.M. Assessing the accuracy and applied use of satellite-derived precipitation estimates over Nepal. *Appl. Geogr.* **2012**, *34*, 626–638.
88. Chen, C.; Yu, Z.; Li, L.; Yang, C. Adaptability evaluation of TRMM satellite rainfall and its application in the Dongjiang River Basin. *Procedia Environ. Sci.* **2011**, *10*, 396–402.
89. Grünzweig, J.M.; Gelfand, I.; Fried, Y.; Yakir, D. Biogeochemical factors contributing to enhanced carbon storage following afforestation of a semi-arid shrubland. *Biogeosciences* **2007**, *4*, 891–904.
90. McDowell, N.; Pockman, W.T.; Allen, C.D.; Breshears, D.D.; Cobb, N.; Kolb, T.; Plaut, J.; Sperry, J.; West, A.; Williams, D.G.; *et al.* Mechanisms of plant survival and mortality during drought: Why do some plants survive while others succumb to drought? *New Phytol.* **2008**, *178*, 719–739.
91. Zhang, L.; Xiao, J.; Li, J.; Wang, K.; Lei, L.; Guo, H. The 2010 spring drought reduced primary productivity in southwestern China. *Environ. Res. Lett.* **2012**, *7*, 045706.

92. Colditz, R.R.; Gessnert, U.; Conradt, C.; van Zyl, D.; Malherbe, J.; Newby, T.; Landmannt, T.; Schmidt, M.; Dech, S. Dynamics of MODIS Time Series for Ecological Applications in Southern Africa. In Proceedings of the 2007 International Workshop on the Analysis of Multi-Temporal Remote Sensing Images, Leuven, Belgium, 18–20 July 2007.
93. Climate Change 2007: Impacts, Adaptation and Vulnerability. Available online: http://www.ipcc.ch/publications_and_data/publications_ipcc_fourth_assessment_report_wg2_report_impacts_adaptation_and_vulnerability.htm (accessed on 10 February 2014).